Dalton Transactions

ROYAL SOCIETY OF CHEMISTRY

PAPER

View Article Online
View Journal

Cite this: DOI: 10.1039/d6dt00545d

Photoactive four-coordinate copper(I) complexes based on chelating diimine, diphosphine, and diisocyanide ligands with high excited-state energies

Tim H. Eggenweiler,[a] Alessandro Prescimone,[b] Daniel Häussinger[a] and Oliver S. Wenger*[a]

Received 5th March 2026,
Accepted 23rd April 2026

DOI: 10.1039/d6dt00545d

rsc.li/dalton

Tetrahedral complexes of copper(I), a more abundant metal than the precious metals traditionally used, have emerged as a suitable alternative in photochemistry and photophysics. While many ligand designs focus on chelating α-diimine and diphosphine ligands, here we report the effect of chelating diisocyanide ligands on photoactive copper(I) complexes. Three new heteroleptic copper(I) complexes are exhibiting photoluminescence at room temperature from a ^{3}MLCT excited state, and a homoleptic isocyanide copper(I) complex luminesces from a ligand-centered state. Among the three new heteroleptic complexes, the one that combines a diphosphine and diisocyanide ligand led to a nearly ideal tetrahedral geometry and an unusually high ^{3}MLCT excited-state energy. This high triplet energy was used in a proof-of-principle upconversion process and triplet–triplet energy transfer photocatalysis. Our findings demonstrate how diisocyanide chelate ligands can be used to tune the photophysical and photochemical properties of photoactive copper(I) complexes with four-coordinate coordination environments.

Introduction

Copper(I) complexes have been a classical workhorse in photophysics, photochemistry,[1–4] and solar cells.[5–8] Many of them are characterized by favorable photophysical properties, such as long luminescence lifetimes as well as high photoluminescence quantum yields due to their closed d^{10} subshell. Early on, tetrahedral copper(I) complexes with α-diimine ligands, like 1,10-phenantroline, were investigated,[9,10] and as an emerging field, trigonal[11–13] and linear[14,15] copper(I) complexes are now increasingly investigated (Fig. 1a).

A key design principle for tetrahedral copper(I) complexes is to introduce steric bulk around the metal center, that the pseudo-Jahn–Teller distortion in the photoactive ^{3}MLCT state can be minimized and long-lived excited-states and good luminescence properties can be achieved.[16,17] Many homoleptic copper(I) complexes are straightforward to synthesize, whereas obtaining heteroleptic complexes is more difficult but can often be achieved if the steric bulk is big enough to prevent coordination of two of the same ligands.[18,19] This synthetic approach provided access to photoactive copper(I) complexes with particularly favorable photophysical and photochemical properties owing to the combination of different ligand classes such as diimines and diphosphines.[20–27]

The foundation for isocyanide ligands in copper(I) complexes was laid by a heteroleptic complex with two monodentate isocyanide ligands.[28] By contrast, diisocyanide chelate ligands are underexplored in photoactive copper(I) complex until now.[29] A recent study reported a copper(I) diisocyanide complex from which no photoluminescence could be detected in solution, and its electronic structure remained largely unexplored.[29] Against this background and based on our own research on photoactive transition metal complexes with chelating diisocyanide ligands,[30–32] we report here a series of homo- and heteroleptic copper(I) complexes, in which we target a high energy for the luminescent ^{3}MLCT state or any other photoactive triplet excited state. High-energy triplet excited states are interesting in the context of synthetic photochemistry to sensitize triplet-energy transfer-based photoreactions[33,34] or for the storage of solar energy in the form of chemical energy.[35–37]

We chose in our work three different ligand classes: diisocyanide, diphosphine and phenanthroline (Fig. 1b), to synthesize and characterize a series of new homo- and heteroleptic copper(I) complexes. We anticipated two opposing effects on the electronic structure of the complexes across this ligand series: (1) as the σ-donation is likely somewhat increased in

[a]Department of Chemistry, University of Basel, St Johanns-Ring 19, 4056 Basel, Switzerland. E-mail: oliver.wenger@unibas.ch
[b]Department of Chemistry, University of Basel, BPR 1096, Mattenstrasse 24a, 4058 Basel, Switzerland

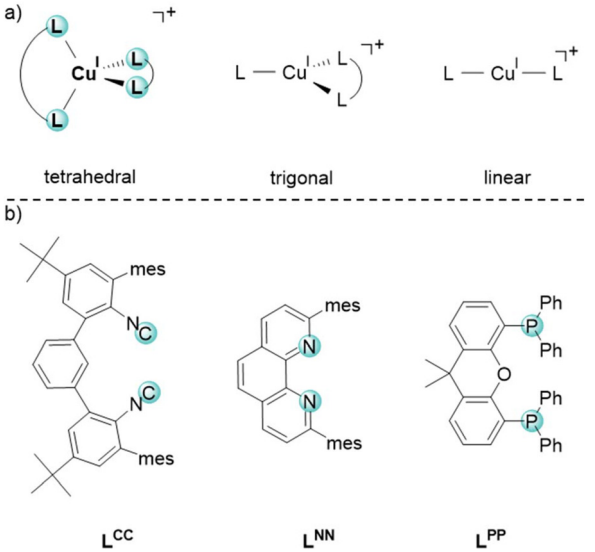

Fig. 1 (a) Representative coordination geometries of photoactive copper(I) complexes. (b) Molecular structures of the bidentate ligands used to form tetrahedral copper(I) complexes in this work: L^{CC}, L^{NN} and L^{PP} (mes = mesityl; Ph = phenyl). Using these three ligands, four new tetrahedral copper(I) complexes were synthesized: $[CuL^{CC}L^{CC}]^+$, $[CuL^{CC}L^{PP}]^+$, $[CuL^{CC}L^{NN}]^+$ and $[CuL^{NN}L^{PP}]^+$.

the diisocyanide and diphosphine ligands compared to phenanthroline, the electron density at the copper(I) center can potentially increase through this effect, which could lead to a stabilization of the copper(II)-like ^{3}MLCT excited state but raise the energy of the metal-based HOMO in the electronic ground state. (2) On the other hand, π-backbonding is expected to increase with the diisocyanide and diphosphine ligands relative to the phenanthroline ligand. Isocyanide ligands can stabilize metals in significantly lower oxidation states than phenanthroline, and this is due to the substantially stronger π-backbonding ability of isocyanides.[38,39] As the electron density of the copper(I) center can decrease through this effect, this could potentially lead to stabilization of the metal-centered orbitals and raise the energy of the photoactive ^{3}MLCT state. It was not prior clear to us which one of the two effects (σ-donation or π-backbonding) is dominant, and hence we anticipated that our study would be able to clarify this and thereby provide fundamental insight into previously unexplored molecular design strategies for photoactive copper(I) complexes.

From the diisocyanide, diphosphine and phenanthroline ligands four new copper(I) complexes, $[CuL^{CC}L^{CC}]^+$, $[CuL^{CC}L^{PP}]^+$, $[CuL^{CC}L^{NN}]^+$ and $[CuL^{NN}L^{PP}]^+$, were synthesized, of which three, $[CuL^{CC}L^{PP}]^+$, $[CuL^{CC}L^{NN}]^+$ and $[CuL^{NN}L^{PP}]^+$, exhibit photoluminescence from a ^{3}MLCT excited state in solution at room temperature. The ligand combination of the diphosphine with the diisocyanide ligand leads to the complex $[CuL^{CC}L^{PP}]^+$, which displays an unusually high ^{3}MLCT energy. Finally, a new homoleptic isocyanide copper(I) complex, $[CuL^{CC}L^{CC}]^+$, was synthesized, which shows ligand-based fluorescence.

Results and discussion

Synthesis and characterization

The two ligands L^{CC} and L^{NN} were synthesized according to published methods,[31,40,41] while L^{PP} is commercially available. From these three ligands the four copper(I) complexes could be synthesized following the so-called HETPHEN (heteroleptic phenanthrolines) approach.[18,19] All four complexes were characterized using ^{1}H and ^{13}C NMR spectroscopy, elemental analysis, and high-resolution mass spectrometry.

In the ^{1}H and ^{13}C NMR spectra, the signals split into two sets for all four copper(I) complexes due to the presence of two different conformers in all four cases. Variable-temperature NMR (VT NMR) spectroscopy was conducted for $[CuL^{CC}L^{PP}]^+$ and reveals a dynamic interconversion between two conformers. We believe a slow oscillating motion of the ligand backbone caused by the increased steric bulk is the reason for this effect, similar to what we found previously for complexes with diisocyanide ligands.[42] This dynamic interconversion is responsible for the relatively broad proton resonances observed at 298 K for this compound. The direct relationship between the two conformers of $[CuL^{CC}L^{PP}]^+$ was further demonstrated by 2D NMR experiments (Fig. S1 and S25). A dissociation of $[CuL^{CC}L^{PP}]^+$ into the two homoleptic complexes, $[CuL^{CC}L^{CC}]^+$ and $[CuL^{PP}L^{PP}]^+$, as seen in similar reported examples,[43] is here not observed, even at higher temperature (398 K). The ^{1}H NMR spectrum of $[CuL^{CC}L^{PP}]^+$ at 398 K differs strongly from the one of the homoleptic complex $[CuL^{CC}L^{CC}]^+$ at 298 K (Fig. S22).

For $[CuL^{NN}L^{PP}]^+$, $[CuL^{CC}L^{NN}]^+$ and $[CuL^{CC}L^{CC}]^+$ two sets of signals are likewise visible in the NMR spectra. However, in these cases the interconversion between different conformers is sufficiently slow on the NMR timescale to yield well-resolved resonances at room temperature. This interconversion between conformers likely arises from restricted rotation or steric hindrance, leading to dynamic processes on the NMR timescale.

Suitable crystals for single crystal X-ray diffraction analysis could be obtained for all four complexes (Fig. 2). The crystal structures show primarily tetrahedral geometry around the copper(I) center. As an indicator for tetrahedral geometry, the tetrahedral parameter τ_4 (Table S8) can be determined (see SI section 7 for the definition of the tetrahedral parameter).[44]

τ_4 is defined such, that it ranges between a value of 1, corresponding to a perfect tetrahedral geometry, and a value of 0, corresponding to a perfect square planar geometry. For $[CuL^{CC}L^{PP}]^+$ this reveals a very high tetrahedral parameter (τ_4 = 0.94), which is close to an ideal tetrahedral structure. This value is significantly higher than those of $[CuL^{NN}L^{PP}]^+$, $[CuL^{CC}L^{NN}]^+$ and $[CuL^{CC}L^{CC}]^+$, as well as many reported photoactive Cu(I) complexes (Table S9).[29,45,46] For $[CuL^{NN}L^{PP}]^+$ (τ_4 = 0.70) and $[CuL^{CC}L^{NN}]^+$ (τ_4 = 0.69), a structure distorted from ideal tetrahedral geometry, a seesaw-like geometry, is observed. This distortion arises from the comparatively small bite angle of phenanthroline in $[CuL^{NN}L^{PP}]^+$ (77°) and $[CuL^{CC}L^{NN}]^+$ (80.7°).

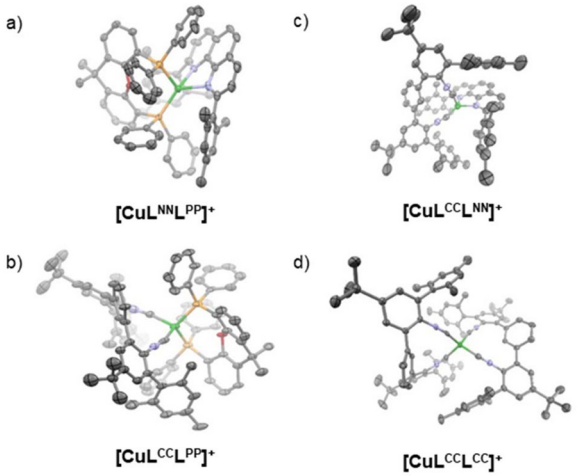

Fig. 2 X-ray crystal structures of the four copper(I) complexes: (a) $[CuL^{NN}L^{PP}]^+$, (b) $[CuL^{CC}L^{PP}]^+$, (c) $[CuL^{CC}L^{NN}]^+$ and (d) $[CuL^{CC}L^{CC}]^+$. Ellipsoids are drawn at 50% probability. Hydrogen atoms and counterions are omitted for clarity. Depth cueing has been applied to enhance structural visualization.

Electrochemical properties

Cyclic voltammetry in MeCN of all four complexes revealed a one-electron oxidation attributed to the $Cu^{I/II}$ redox couple. The trend in oxidation potential (Table 1), determined from the peak current, is: $[CuL^{CC}L^{CC}]^+$ (0.65 V *vs.* SCE) < $[CuL^{CC}L^{PP}]^+$ (0.70 V *vs.* SCE) < $[CuL^{CC}L^{NN}]^+$ (0.86 V *vs.* SCE) < $[CuL^{NN}L^{PP}]^+$ (1.13 V *vs.* SCE). All four complexes show irreversible oxidation, which can be also observed in similar copper(I) complexes.[47–50] The increase in oxidation potential along this series is compatible with decreasing electron density at the Cu(I) center. This in turn can be interpreted in terms of the oxidation potential being primarily influenced by the σ-donation of the ligands. Accordingly, the observed trend is consistent with a decrease in σ-donor strength in the order $L^{CC} > L^{PP} > L^{NN}$, leading to the lowest oxidation potential for $[CuL^{CC}L^{CC}]^+$ and the highest oxidation potential for $[CuL^{NN}L^{PP}]^+$.

Furthermore, this trend is in accordance with reported copper(I) complexes,[29,47–50] for example [Cu(dpp)(binc)]$^+$ (dpp = 2,9-diphenyl-1,10-phenanthroline; binc = bis(2-isocyanophenyl) phenylphosphonate) with an oxidation potential of 0.69 V *vs.* SCE (ref. 29) comparable to $[CuL^{CC}L^{NN}]^+$ (0.86 V *vs.* SCE) or [Cu(dmp)(xantphos)]$^+$ (dmp = 2,9-dimethyl-1,10-phenanthroline; xantphos = (9,9-dimethyl-9*H*-xanthene-4,5-diyl)bis(diphenylphosphane)) with an oxidation potential of 1.21 V *vs.* SCE (ref. 48) comparable to $[CuL^{NN}L^{PP}]^+$ (1.13 V *vs.* SCE). We conclude that the σ-donation effect mentioned in the introduction is dominant here.

Photophysical studies

Photoexcitation into the MLCT absorption band of $[CuL^{NN}L^{PP}]^+$ (λ_{exc} = 430 nm) band leads to an emission at 540 nm in THF at room temperature, comparable to reported structurally similar copper(I) complexes (Fig. 3).[50,51] In $[CuL^{CC}L^{PP}]^+$ the emission is blue shifted compared to $[CuL^{NN}L^{PP}]^+$, indicating a higher-energy emissive excited state for $[CuL^{CC}L^{PP}]^+$. As the luminescence band shape is similar in $[CuL^{NN}L^{PP}]^+$ and $[CuL^{CC}L^{PP}]^+$, it seems plausible that the emission originates from a ^{3}MLCT excited state in both cases. The emission blue-shift observed when replacing L^{NN} by L^{CC} on the $[CuL^{PP}]^+$ fragment is at first glance surprising, given the energetic destabilization of the metal-centered HOMO when going from $[CuL^{NN}L^{PP}]^+$ to $[CuL^{CC}L^{PP}]^+$ found by cyclic voltammetry. Thus, it seems that the energy of the ligand-centered LUMO is raised to an even greater extent than the metal-centered HOMO, which seems plausible because the *m*-terphenyl backbone of the L^{CC} ligand is overall less π-conjugated than the phenanthroline backbone of L^{NN}.

$[CuL^{CC}L^{NN}]^+$ does not show emission in THF at room temperature (Fig. S7) but luminesces in non-coordinating DCM with a band maximum at 630 nm and a band shape compatible with ^{3}MLCT emission also in this case. The lack of emission in THF could be due to the slightly coordinating nature of this solvent and the presence of a diisocyanide ligand that is less rigid and less bulky in comparison to the conventionally used diphosphines. The emission redshift compared to $[CuL^{NN}L^{PP}]^+$ when exchanging L^{PP} with L^{CC} on the $[CuL^{NN}]^+$ fragment can be understood on the basis that the phenanthroline-centered LUMO remains essentially constant in energy, whereas the metal-centered HOMO increases in energy when going from $[CuL^{NN}L^{PP}]^+$ to $[CuL^{CC}L^{NN}]^+$, as manifested by the decrease in oxidation potential reported above.

The luminescence of $[CuL^{CC}L^{CC}]^+$ is markedly blue shifted with respect to the three heteroleptic complexes and its band shape is significantly different than in the homoleptic complexes and furthermore resembles the lowest-energy absorption band of the $[CuL^{CC}L^{CC}]^+$ complex. On this basis, the luminescence of $[CuL^{CC}L^{CC}]^+$ is assigned to an electronic transition dominated by ligand-centered character. A direct comparison with the fluorescence spectrum of L^{CC} is not meaningful, as the uncoordinated isocyanide carbon atom of the free ligand influences the photophysical properties.[52] We conclude that in the $[CuL^{CC}L^{CC}]^+$ complex, the lowest MLCT excited states appear to be shifted to substantially higher energies, presumably due to the weaker overall π-conjugation of the diisocyanide ligand.

Photoluminescence quantum yield measurements in solution are complicated by photodegradation occurring while irradiating $[CuL^{NN}L^{PP}]^+$ and $[CuL^{CC}L^{NN}]^+$ (Fig. S5 and S7). This may arise from partial (or full) detachment of one ligand in solution or displacement of one ligand with a solvent molecule.[53] This behaviour is not observed in solid state (Fig. S11), and therefore we focused on photoluminescence quantum yield measurements for the ^{3}MLCT emission of $[CuL^{NN}L^{PP}]^+$, $[CuL^{CC}L^{PP}]^+$ and $[CuL^{CC}L^{NN}]^+$ in the solid state. The photoluminescence quantum yield (Φ) in the solid-state decreases from $[CuL^{NN}L^{PP}]^+$ (50.6%) to $[CuL^{CC}L^{NN}]^+$ (8.3%) and $[CuL^{CC}L^{PP}]^+$ (1.5%). The observed trend appears to arise from a complex interplay between excited-state energy and concentration quenching. On the one hand, according to the energy-gap law, intrinsic nonradiative relaxation for individual complexes decreases as the excited-state energy increases. On the

other hand, higher excited-state energy may enhance concentration-quenching pathways, offsetting this intrinsic advantage.

Going back to the solution state, $[CuL^{NN}L^{PP}]^+$, $[CuL^{CC}L^{NN}]^+$ and $[CuL^{CC}L^{CC}]^+$ exhibit mono-exponential luminescence decays (Fig. S4, S8 and S10), whereas $[CuL^{CC}L^{PP}]^+$ exhibits a bi-exponential decay due to the presence of two conformers. Here we will focus on the lifetime of the longer-lived conformer (τ = 4.45 μs), as this displays the major contribution (81%) to the luminescence decay, whereas the conformer with the shorter excited-state lifetime (τ = 0.39 μs) contributes with only 19% (Fig. S6). Furthermore, the photodegradation products of $[CuL^{CC}L^{PP}]^+$ and $[CuL^{CC}L^{NN}]^+$ also emit, resulting in a multi-exponential decay in solution (Fig. S5 and S7). For $[CuL^{CC}L^{CC}]^+$, the short luminescence lifetime (τ = 9.9 ns) (Fig. S10) together with the band shape (Fig. 3) agrees with a fluorescence emission from a ligand centered singlet excited state. We did not find any evidence for a longer-lived triplet excited state by transient absorption spectroscopy and therefore assume that the fluorescent excited state undergoes very inefficient intersystem crossing in this case, presumably because it contains limited metal-character.

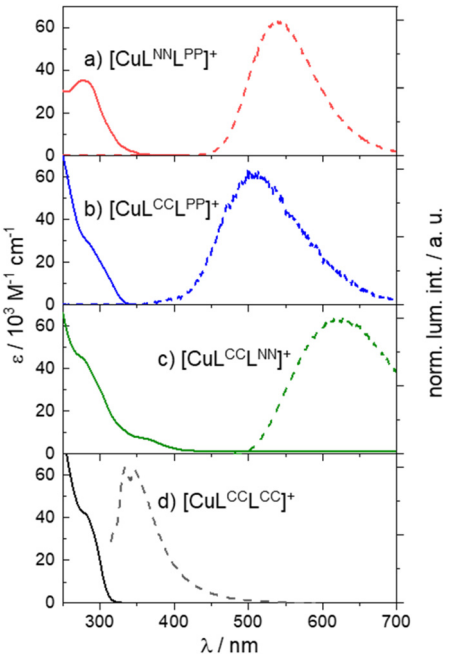

Fig. 3 UV/Vis absorption spectra (solid lines) and emission spectra (dashed lines) of the four copper(I) complexes. $[CuL^{CC}L^{CC}]^+$, $[CuL^{CC}L^{PP}]^+$, and $[CuL^{NN}L^{PP}]^+$ were measured in dry, deaerated THF, $[CuL^{CC}L^{NN}]^+$ was measured in dry, deaerated DCM. Emission spectra were recorded at 100 μM and normalized to the maximum intensity. $[CuL^{CC}L^{PP}]^+$ was excited with a 355 nm laser (20 mJ; 10 ns pulse width; 1 μs integration time) and the luminescence was recorded with a time-gated delay of 500 ns. The other three complexes were excited using continuous irradiation: $[CuL^{NN}L^{PP}]^+$ at 430 nm, $[CuL^{CC}L^{NN}]^+$ at 370 nm and $[CuL^{CC}L^{CC}]^+$ at 300 nm.

The ^{3}MLCT lifetime of $[CuL^{NN}L^{PP}]^+$ (τ = 16.3 μs), and the magnitude of this lifetime is in agreement with other reported examples of heteroleptic complexes with diimine and diphosphine ligands.[47,51] The shorter lifetime of τ = 4.45 μs in deaerated THF for $[CuL^{CC}L^{PP}]^+$, despite the blue shifted ^{3}MLCT emission, is most likely due to the more flexible isocyanide backbone of L^{CC} compared to L^{NN}, leading to more distortion of the excited state, and therefore more non-radiative pathways seem to be present. This effect seems to be also present for $[CuL^{CC}L^{NN}]^+$, as a short lifetime of τ = 219 ns in deaerated DCM was measured.

The ^{3}MLCT excited state energy (labelled E_{00} in Table 1) was estimated at 10% of the high-energy onset of the emission spectra, providing values of 2.95 eV for $[CuL^{CC}L^{PP}]^+$, 2.65 eV for $[CuL^{NN}L^{PP}]^+$, and 2.44 eV for $[CuL^{CC}L^{NN}]^+$. For $[CuL^{CC}L^{CC}]^+$, as explained above, we observe ligand-based fluorescence, and there is no evidence for significant population of the T_1 excited state. Based on the fluorescence spectrum of $[CuL^{CC}L^{PP}]^+$, the energy of the S_1 excited state was estimated to be around 3.9 eV.

Among the four complexes investigated, $[CuL^{CC}L^{PP}]^+$ displays particularly favourable properties, in that it features a comparatively low oxidation potential (E_{ox} = 0.70 V *vs.* SCE), an unusually high triplet energy (E_{00} = 2.95 eV), and a relatively long ^{3}MLCT lifetime (4.45 μs for the predominant conformer). These properties lead to an estimated excited-state oxidation

Table 1 Summary of the photophysical and electrochemical properties of Cu^I complexes

Entry	Compound	$\lambda_{max,\,em}$ [nm] (Φ [%])			τ_0 [μs]		E_{00} [eV]	E_{ox} [V. *vs.* SCE]	E^*_{ox} [V. *vs.* SCE]
		THF[a]	DCM[a]	Powder[d]	THF[a]	DCM[a]	—	MeCN[a]	—
1	$[CuL^{NN}L^{PP}]^+$	540		540 (50.6)	16.3		2.65	1.13	−1.52
2	$[CuL^{CC}L^{PP}]^+$	(350)[b] 510		475 (1.5)	0.39[c] 4.45[c]		2.95	0.70	−2.25
3	$[CuL^{CC}L^{NN}]^+$		(415)[b] 630	540 (8.3)		(0.007)[b] (0.0011)[b] 0.219	2.44	0.86	−1.58
4	$[CuL^{CC}L^{CC}]^+$	332		—	0.0099		—	0.65	—

[a] In dry, deaerated solvent at 20 °C. [b] Emission assigned to a photodegradation product. [c] Biexponential emission decay tentatively assigned to the two different, slowly interconverting conformers as seen in the variable-temperature NMR studies. [d] Solid-state measurement at 20 °C. $\lambda_{max,\,em}$, wavelength of the emission band maximum; τ_0, lifetime of the photoactive excited state. E_{00} was estimated from 10% of the high-energy onset of the emission spectrum; E_{ox} oxidation potential referenced against SCE; estimated E^*_{ox} oxidation potential in the photoactive ^{3}MLCT excited state referenced against SCE; Φ photoluminescence quantum yield in the solid state at room temperature.

potential E^*_{ox} of −2.25 V *vs.* SCE, potentially making $[CuL^{CC}L^{PP}]^+$, a strong excited-state reductant,[29,48,51,54,55] in addition to a potent triplet energy donor. In the following, that latter aspect will be in focus.

Sensitized triplet–triplet annihilation upconversion

Among the three heteroleptic complexes investigated herein and compared to many previously reported tetrahedral copper (I) complexes,[2] $[CuL^{CC}L^{PP}]^+$ displays a high ^{3}MLCT excited-state energy (Table 1). This complex was therefore used in a triplet–triplet energy transfer (TTET) experiment with 4,4′-dimethoxy-1,1′-biphenyl (**BP**), in which the lowest triplet excited state (T_1) is 2.74 eV above the electronic ground state.[56] Irradiating $[CuL^{CC}L^{PP}]^+$ in the presence of 25 mM **BP** results in a triplet–triplet energy transfer (TTET) (Fig. 4a) forming the lowest triplet excited state of **BP** (^{3}**BP***). The ^{3}**BP*** species can be observed directly in the transient absorption spectrum (Fig. 4b), where a new band with a maximum at 393 nm arises, which matches recently reported examples of triplet biphenyl species.[56] The lifetime of the desired ^{3}**BP*** photoproduct in deaerated THF at room temperature is 149 μs (Fig. S14).

Expectedly, the ^{3}MLCT emission of $[CuL^{CC}L^{PP}]^+$ observed in the absence of **BP** (Fig. S13), is quenched by **BP** in the transient absorption spectrum (Fig. 4b).[56] The luminescence quenching rate constant could not be determined, because the emission of the photodegradation product discussed in the previous section overlaps with the emission from $[CuL^{CC}L^{PP}]^+$. This becomes increasingly problematic at higher concentrations of **BP**, as the ^{3}MLCT emission of $[CuL^{CC}L^{PP}]^+$ is quenched, but the emission of the photodegradation product remains seemingly unaffected. The main conclusion from this series of experiments is that the unusually high triplet excited state energy of $[CuL^{CC}L^{PP}]^+$ is confirmed by the TTET process to **BP**.

Following the triplet–triplet energy transfer (TTET), two ^{3}**BP*** species undergo triplet–triplet annihilation (TTA) (Fig. 4c), resulting in the population of the S_1 state of **BP** at 3.97 eV (ref. 56) and delayed fluorescence from that state with a band maximum at 347 nm (purple part of Fig. 4d). The upconversion luminescence spectrum of **BP** is identical to that obtained upon direct **BP** excitation,[57] but is still detectable after 100 μs delay time, which confirms the delayed nature of the upconversion fluorescence reflecting the ^{3}**BP*** lifetime. For reference, the prompt fluorescence of **BP** obtained after direct UV excitation is 11 ns.[56,57] Additionally, back energy transfer from **BP** to $[CuL^{CC}L^{PP}]^+$ is observed as a long-lived lumine-

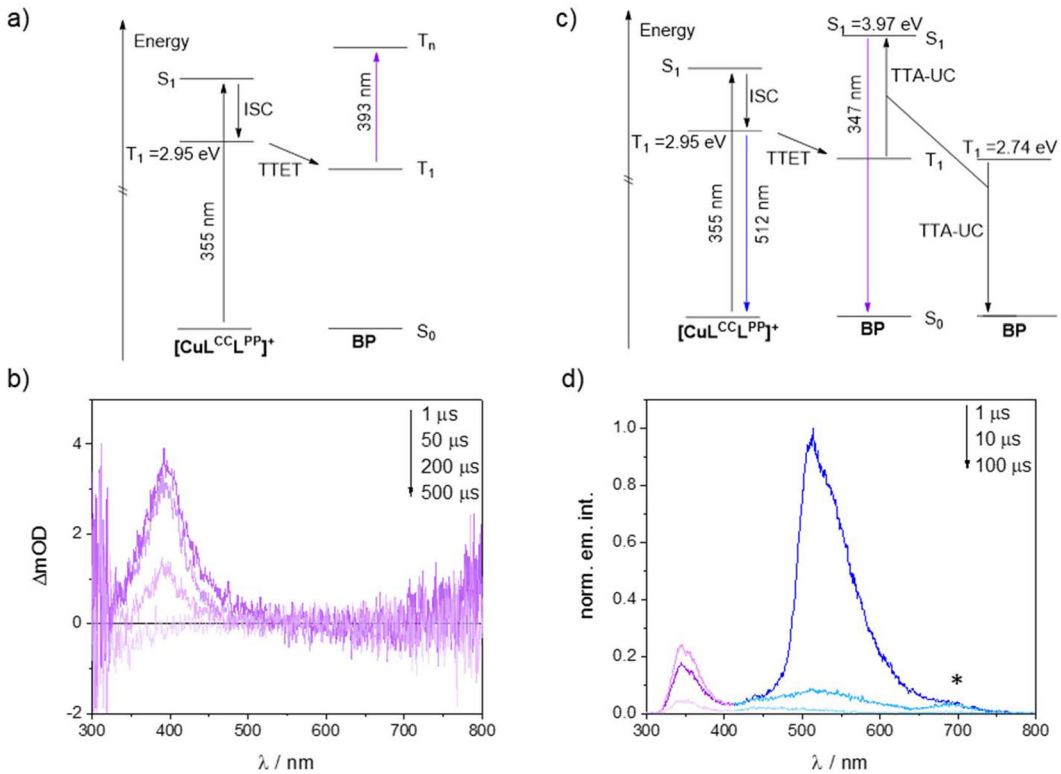

Fig. 4 Triplet–triplet energy transfer (TTET) experiment using 100 μM $[CuL^{CC}L^{PP}]^+$ and 25 mM 4,4′-dimethoxy-1,1′-biphenyl (**BP**) in deaerated THF. Excitation was performed at 355 nm (25 mJ; 10 ns pulse width). Detection occurred with a 1 μs integration time. (a) Jablonski diagram illustrating excitation and relaxation pathways of the TTET relevant to the (b) transient absorption spectrum measured with different time delays (1 to 500 μs). (c) Jablonski diagram illustrating excitation, triplet–triplet annihilation upconversion (TTA-UC) and relaxation pathways of the TTET and TTA-UC relevant to the (d) emission spectrum measured with different time delays (1 to 100 μs). The asterisk indicates the second harmonic of the upconverted emission of **BP**.

scence signal at 500 nm (blue marked part of Fig. 4d). This confirms our expectation (Fig. 4c) that the triplet energies of the $[CuL^{CC}L^{PP}]^+$ donor and the **BP** acceptor are close in energy, such that the long-lived ^{3}**BP*** state can repopulate the luminescent ^{3}MLCT excited state of $[CuL^{CC}L^{PP}]^+$. Typically, this is the case when the donor–acceptor energy gap is on the order of 0.2 eV or less.[58]

The main finding of this section is that the high ^{3}MLCT energy of $[CuL^{CC}L^{PP}]^+$ is confirmed by the TTET experiments and the upconversion studies. The upconversion process itself is not the primary focus of this work and exhibits a comparatively small anti Stokes shift and low efficiency. As a result, a detailed photophysical characterization of the upconversion mechanism was not feasible within the scope of this study.

Triplet–triplet energy transfer photocatalysis

To explore the application potential of $[CuL^{CC}L^{PP}]^+$ in triplet–triplet energy transfer photocatalysis, the intramolecular [2 + 2] cycloaddition of norbornadiene to quadricyclane (Fig. 5a), a molecular solar thermal energy storage (MOST) system, was chosen.[37,59,60] Norbornadiene exhibits a triplet energy of 2.7 eV, and $[CuL^{CC}L^{PP}]^+$ should therefore be able to sensitize this triplet excited state and catalyze the photoisomerization reaction of norbornadiene to quadricyclane. The reaction was monitored by ^{1}H-NMR spectroscopy as a function of continuous irradiation at 365 nm (Fig. 5b) and over time, the proton resonance of norbornadiene at 1.94 ppm (red) gets smaller and three new resonances corresponding to quadricyclane (green) increase. After two hours of reaction time a yield of 59% was observed with $[CuL^{CC}L^{PP}]^+$, whereas only minor turnover (4%) occurred without a photocatalyst (Fig. S3).

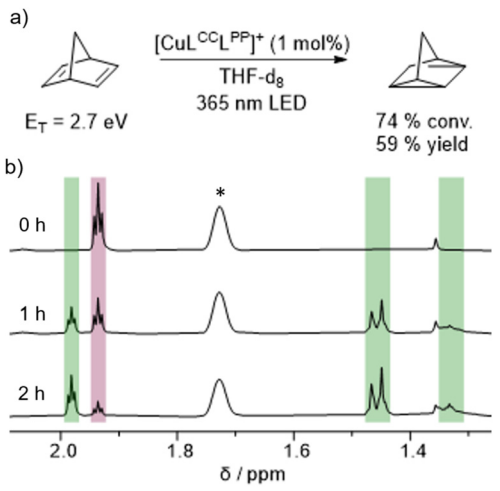

Fig. 5 (a) [2 + 2] Cycloaddition of norbornadiene to quadricyclane in deaerated THF-d_8. Starting material conversion and product yield were determined by ^{1}H-NMR spectroscopy using trimethyl(phenyl)silane as an internal standard. (b) ^{1}H-NMR spectra (aliphatic region) of the reaction mixture. Signals corresponding to norbornadiene (starting material) are highlighted in red, and those of quadricyclane (product) are highlighted in green. The signal marked with an asterisk (*) originates from residual non-deuterated THF present in THF-d_8.

Conclusions

Tetrahedral copper(I) complexes play a central role in photophysics and photochemistry with favourable properties of long luminescence lifetimes and high quantum yields, with many previous studies focusing on phenanthroline and diphosphine ligands.[1–4] Our work aimed to increase the triplet energy of copper(I) complexes through diisocyanide chelate ligands and achieve fundamental insights for the design principles of photoactive copper(I) complexes beyond the traditionally used α-diimine and diphosphine ligands.

The metal-based HOMO is destabilized when going from phenanthroline to diphosphine to diisocyanide, as seen in the markedly lowered oxidation potential when going from $[CuL^{CC}L^{NN}]^+$ to $[CuL^{CC}L^{PP}]^+$ and $[CuL^{CC}L^{CC}]^+$, or when comparing $[CuL^{NN}L^{PP}]^+$ and $[CuL^{CC}L^{NN}]^+$. This suggests that σ-donation effects outweigh π-backbonding effects as far as the HOMO energy is concerned. At the same time, the energy of the ligand-based LUMO increases across the abovementioned ligand series, presumably due to decreasing π-conjugation in the ligand backbone in the series $L^{NN} > L^{PP} > L^{CC}$. In the $[CuL^{CC}L^{PP}]^+$ complex, this leads to a luminescent ^{3}MLCT excited state with a markedly higher energy than in many known photoactive copper(I) complexes.[29,48,51,54,55] Proof-of-principle upconversion and triplet–triplet energy transfer photocatalysis experiments illustrate the usefulness of the unusually high-energy ^{3}MLCT excited state of $[CuL^{CC}L^{PP}]^+$. The upper limit of our design approach is reached in the homoleptic $[CuL^{CC}L^{CC}]^+$ diisocyanide copper(I) complex, where a ligand-centered excited state becomes photoactive.

In summary, our work illustrates how diisocyanide chelate ligands can be used to tune the photophysical and photochemical properties of photoactive copper(I) complexes with four-coordinate coordination environments.

Author contributions

T. H. E. conceptualization, data curation, formal analysis, investigation, visualization, writing – original draft, writing – review & editing; D. H. and A. P. data curation, formal analysis; O. S. W. funding acquisition, project administration, writing – review & editing.

Conflicts of interest

There are no conflicts to declare.

Data availability

The supporting data has been provided as part of the supplementary information (SI). Supplementary information: NMR spectra, solid state emission spectra, photoluminescence lifetime measurements, crystallographic details and further experimental details. See DOI: https://doi.org/10.1039/d6dt00545d.

CCDC 2502158–2502161 contain the supplementary crystallographic data for this paper.[61a–d]

Acknowledgements

Financial support from the University of Basel is acknowledged.

References

1 A. Hossain, A. Bhattacharyya and O. Reiser, *Science*, 2019, **364**, eaav9713.
2 J. Beaudelot, S. Oger, S. Perusko, T. A. Phan, T. Teunens, C. Moucheron and G. Evano, *Chem. Rev.*, 2022, **122**, 16365–16609.
3 T. Y. Li, S. J. Zheng, P. I. Djurovich and M. E. Thompson, *Chem. Rev.*, 2024, **124**, 4332–4392.
4 F. N. Castellano and M. C. Rosko, *Acc. Chem. Res.*, 2024, **57**, 2872–2886.
5 D. Di, A. S. Romanov, L. Yang, J. M. Richter, J. P. Rivett, S. Jones, T. H. Thomas, M. Abdi Jalebi, R. H. Friend, M. Linnolahti, M. Bochmann and D. Credgington, *Science*, 2017, **356**, 159–163.
6 R. Hamze, J. L. Peltier, D. Sylvinson, M. Jung, J. Cardenas, R. Haiges, M. Soleilhavoup, R. Jazzar, P. I. Djurovich, G. Bertrand and M. E. Thompson, *Science*, 2019, **363**, 601–606.
7 P. J. Conaghan, C. S. B. Matthews, F. Chotard, S. T. E. Jones, N. C. Greenham, M. Bochmann, D. Credgington and A. S. Romanov, *Nat. Commun.*, 2020, **11**, 1758.
8 L. E. Burmeister, F. Doettinger, K. J. Haseloff, C. Kleeberg, M. Boujtita, S. Pascal, F. Odobel, S. Tschierlei, Y. Pellegrin and M. Karnahl, *JACS Au*, 2025, **5**, 3960–3973.
9 M. W. Blaskie and D. R. McMillin, *Inorg. Chem.*, 1980, **19**, 3519–3522.
10 C. O. Dietrich-Buchecker, P. A. Marnot, J.-P. Sauvage, J. R. Kirchhoff and D. R. McMillin, *J. Chem. Soc., Chem. Commun.*, 1983, **9**, 513–515.
11 D. Kim, M. C. Rosko, F. N. Castellano, T. G. Gray and T. S. Teets, *J. Am. Chem. Soc.*, 2024, **146**, 19193–19204.
12 S. Chakraborty, K. Agyekum, D. Kim and T. S. Teets, *Chem. Sci.*, 2025, **16**, 22527–22535.
13 L. E. Burmeister, L. J. Groth, P. R. Meinhold, J. P. Zurwellen, D. Bockfeld, R. Frank, M. Karnahl, M. Tamm and S. Tschierlei, *JACS Au*, 2025, **5**, 2792–2801.
14 M. Gernert, L. Balles-Wolf, F. Kerner, U. Muller, A. Schmiedel, M. Holzapfel, C. M. Marian, J. Pflaum, C. Lambert and A. Steffen, *J. Am. Chem. Soc.*, 2020, **142**, 8897–8909.
15 C. N. Muniz, C. A. Archer, J. S. Applebaum, A. Alagaratnam, J. Schaab, P. I. Djurovich and M. E. Thompson, *J. Am. Chem. Soc.*, 2023, **145**, 13846–13857.
16 C. E. McCusker and F. N. Castellano, *Inorg. Chem.*, 2013, **52**, 8114–8120.
17 S. Garakyaraghi, C. E. McCusker, S. Khan, P. Koutnik, A. T. Bui and F. N. Castellano, *Inorg. Chem.*, 2018, **57**, 2296–2307.
18 M. Schmittel and A. Ganz, *Chem. Commun.*, 1997, **11**, 999–1000.
19 M. Schmittel, U. Lüning, M. Meder, A. Ganz, C. Michel and M. Herderich, *Heterocycl. Commun.*, 1997, **3**, 493–498.
20 D. G. Cuttell, S. M. Kuang, P. E. Fanwick, D. R. McMillin and R. A. Walton, *J. Am. Chem. Soc.*, 2002, **124**, 6–7.
21 S. M. Kuang, D. G. Cuttell, D. R. McMillin, P. E. Fanwick and R. A. Walton, *Inorg. Chem.*, 2002, **41**, 3313–3322.
22 C. Minozzi, A. Caron, J. C. Grenier-Petel, J. Santandrea and S. K. Collins, *Angew. Chem., Int. Ed.*, 2018, **57**, 5477–5481.
23 S. Keller, A. Prescimone, M. G. La Placa, J. M. Junquera-Hernández, H. J. Bolink, E. C. Constable, M. Sessolo, E. Ortí and C. E. Housecroft, *RSC Adv.*, 2020, **10**, 22631–22644.
24 C. E. Housecroft and E. C. Constable, *J. Mater. Chem. C*, 2022, **10**, 4456–4482.
25 L. Kohler, D. Hayes, J. Hong, T. J. Carter, M. L. Shelby, K. A. Fransted, L. X. Chen and K. L. Mulfort, *Dalton Trans.*, 2016, **45**, 9871–9883.
26 M. C. Rosko, J. P. Wheeler, R. Alameh, A. P. Faulkner, N. Durand and F. N. Castellano, *Inorg. Chem.*, 2024, **63**, 1692–1701.
27 A. Olding, L. Cameron, L. N. Pham, J. P. Shephard, N. T. Lucas, S. A. Moggach, M. Massi, T. U. Connell, C. C. Ho, M. L. Coote and A. C. Bissember, *ACS Catal.*, 2025, **15**, 3731–3740.
28 C. S. Smith and K. R. Mann, *J. Am. Chem. Soc.*, 2012, **134**, 8786–8789.
29 M. Knorn, T. Rawner, R. Czerwieniec and O. Reiser, *ACS Catal.*, 2015, **5**, 5186–5193.
30 L. A. Büldt, X. Guo, A. Prescimone and O. S. Wenger, *Angew. Chem., Int. Ed.*, 2016, **55**, 11247–11250.
31 N. Sinha, C. Wegeberg, D. Häussinger, A. Prescimone and O. S. Wenger, *Nat. Chem.*, 2023, **15**, 1730–1736.
32 T. Jin, N. Sinha, D. S. Wagner, A. Prescimone, D. Haussinger and O. S. Wenger, *J. Am. Chem. Soc.*, 2025, **147**, 4587–4594.
33 F. Strieth-Kalthoff, M. J. James, M. Teders, L. Pitzer and F. Glorius, *Chem. Soc. Rev.*, 2018, **47**, 7190–7202.
34 Q. Q. Zhou, Y. Q. Zou, L. Q. Lu and W. J. Xiao, *Angew. Chem., Int. Ed.*, 2019, **58**, 1586–1604.
35 L. Dong, Y. Feng, L. Wang and W. Feng, *Chem. Soc. Rev.*, 2018, **47**, 7339–7368.
36 Z. Wang, H. Hölzel and K. Moth-Poulsen, *Chem. Soc. Rev.*, 2022, **51**, 7313–7326.
37 T. J. B. Zähringer, N. Perez Lopez, R. Schulte, M. Schmitz, H. Ihmels and C. Kerzig, *Angew. Chem., Int. Ed.*, 2025, **64**, e202414733.
38 N. Sinha, C. Wegeberg, D. Häussinger, A. Prescimone and O. S. Wenger, *Nat. Chem.*, 2023, **15**, 1730–1736.

39 C. C. Scarborough, S. Sproules, T. Weyhermüller, S. DeBeer and K. Wieghardt, *Inorg. Chem.*, 2011, **50**, 12446–12462.
40 L. Kohler, D. Hayes, J. Hong, T. J. Carter, M. L. Shelby, K. A. Fransted, L. X. Chen and K. L. Mulfort, *Dalton Trans.*, 2016, **45**, 9871–9883.
41 T. Rawner, E. Lutsker, C. A. Kaiser and O. Reiser, *ACS Catal.*, 2018, **8**, 3950–3956.
42 C. Wegeberg, D. Häussinger, S. Kupfer and O. S. Wenger, *J. Am. Chem. Soc.*, 2024, **146**, 4605–4619.
43 A. Kaeser, M. Mohankumar, J. Mohanraj, F. Monti, M. Holler, J.-J. Cid, O. Moudam, I. Nierengarten, L. Karmazin-Brelot, C. Duhayon, B. Delavaux-Nicot, N. Armaroli and J. F. Nierengarten, *Inorg. Chem.*, 2013, **52**, 12140–12151.
44 L. Yang, D. R. Powell and R. P. Houser, *Dalton Trans.*, 2007, 955–964.
45 F. Xu, T. Tao, K. Zhang, X. X. Wang, W. Huang and X. Z. You, *Dalton Trans.*, 2013, **42**, 3631–3645.
46 Y. Yang, F. Doettinger, C. Kleeberg, W. Frey, M. Karnahl and S. Tschierlei, *Front. Chem.*, 2022, **10**, 936863.
47 E. Mejía, S. P. Luo, M. Karnahl, A. Friedrich, S. Tschierlei, A. E. Surkus, H. Junge, S. Gladiali, S. Lochbrunner and M. Beller, *Chem. – Eur. J.*, 2013, **19**, 15972–15978.
48 C. Li, R. Dickson, N. Rockstroh, J. Rabeah, D. B. Cordes, A. M. Z. Slawin, P. Hünemörder, A. Spannenberg, M. Bühl, E. Mejía, E. Zysman-Colman and P. C. J. Kamer, *Catal. Sci. Technol.*, 2020, **10**, 7745–7756.
49 L. Zheng, Q. Jiang, H. Bao, B. Zhou, S. P. Luo, H. Jin, H. Wu and Y. Liu, *Org. Lett.*, 2020, **22**, 8888–8893.
50 I. Nohara, C. Wegeberg, M. Devereux, A. Prescimone, C. E. Housecroft and E. C. Constable, *J. Mater. Chem. C*, 2022, **10**, 3089–3102.
51 F. Doettinger, C. Kleeberg, C. Queffélec, S. Tschierlei, Y. Pellegrin and M. Karnahl, *Catal. Sci. Technol.*, 2023, **13**, 4092–4106.
52 P. Herr, C. Kerzig, C. B. Larsen, D. Häussinger and O. S. Wenger, *Nat. Chem.*, 2021, **13**, 956–962.
53 O. Green, B. A. Gandhi and J. N. Burstyn, *Inorg. Chem.*, 2009, **48**, 5704–5714.
54 R. Czerwieniec, J. Yu and H. Yersin, *Inorg. Chem.*, 2011, **50**, 8293–8301.
55 C. Bruschi, X. Gui, N. Salaeh-arae, T. Barchi, O. Fuhr, S. Lebedkin, W. Klopper and C. Bizzarri, *Eur. J. Inorg. Chem.*, 2021, **2021**, 4074–4084.
56 M. Montalti, A. Credi, L. Prodi and M. T. Gandolfi, *Handbook of Photochemistry*, Taylor & Francis, 3rd edn., 2006.
57 R. Jakubowski, A. Januszko, R. William Tilford, G. J. Radziszewski, A. Pietrzak, V. G. Young Jr and P. Kaszyński, *Chem. – Eur. J.*, 2023, **29**, e202203948.
58 J. Wellauer, B. Pfund, I. Becker, F. Meyer, A. Prescimone and O. S. Wenger, *J. Am. Chem. Soc.*, 2025, **147**, 8760–8768.
59 G. S. Hammond, N. J. Turro and A. Fischer, *J. Am. Chem. Soc.*, 1961, **83**, 4674–4675.
60 D. P. Schwendiman and C. Kutal, *J. Am. Chem. Soc.*, 1977, **99**, 5677–5682.
61 (*a*) CCDC 2502158: Experimental Crystal Structure Determination, 2026, DOI: 10.5517/ccdc.csd.cc2pzps5; (*b*) CCDC 2502159: Experimental Crystal Structure Determination, 2026, DOI: 10.5517/ccdc.csd.cc2pzpt6; (*c*) CCDC 2502160: Experimental Crystal Structure Determination, 2026, DOI: 10.5517/ccdc.csd.cc2pzpv7; (*d*) CCDC 2502161: Experimental Crystal Structure Determination, 2026, DOI: 10.5517/ccdc.csd.cc2pzpw8.